Optical properties of liquid carbon measured by femtosecond spectroscopy

D. H. Reitze,* H. Ahn, and M. C. Downer
Physics Department, The University of Texas at Austin, Austin, Texas, 78712
(Received 2 August 1991)

A comprehensive report of femtosecond time-resolved reflectivity and transmission of graphite and diamond following optical excitation above critical melting fluences F_m of 0.13 and 0.63 J/cm^2, respectively, is presented. Normal- and oblique-incidence reflectivity has been measured with 100-fs resolution at wavelengths ranging from 700 to 310 nm. Within 1 ps following excitation above F_m, probe reflectance increases sharply at visible frequencies, remains nearly unchanged at near-ultraviolet frquencies, and depends weakly on excitation fluence. These optical changes are interpreted as an ultrafast melting transition from crystalline graphite or diamond to a common, more reflective liquid state. During the first picosecond following excitation, electron and lattice temperatures substantially equilibrate, and the lattice melts, before heat conducts out of the absorbing volume or the surface hydrodynamically expands. A Drude model of the reflectance spectrum 1 ps after excitation reveals a strongly damped plasma (plasma frequency-relaxation time product $\omega_p\tau\sim 1$), in contrast to liquid silicon ($\omega_p\tau\sim 5$). Inferred electron mean free paths approach the average interatomic spacing (2 Å), implying electron localization. Optically determined dc resistivities up to 625 ± 75 $\mu\Omega$ cm agree with measurements at kilobar ambient pressure, but significantly exceed resistivities measured and calculated at low pressure. Thus, the attribution "metal" is questionable for fluid carbon under these conditions. The results demonstrate that femtosecond lasers can extend condensed-matter thermophysics measurements to temperature-pressure regimes inaccessible by other methods.

I. INTRODUCTION

Scientific debate over the properties of the elusive liquid state of carbon, nature's most refractory material, dates back to Ludwig's[1] 1902 report of increased resistance in carbon rods melted at high pressure. Extensive recent research[2–20] on high temperature-pressure phases of carbon, which has been reviewed by Bundy,[2] reflects not only the wide-ranging importance of the problem in condensed matter physics,[2] astrophysics,[16] and geology,[17–19] but the continuing controversy over the basic properties of the liquid state. For example, much recent debate has focused on whether liquid carbon is metallic or insulating, and on how its electrical conductivity depends on temperature and pressure.[4–14] Much of the controversy stems from the difficulty of creating and studying a reproducible sample of liquid carbon in the laboratory, particularly producing identical samples and conditions by different methods. Since the melting temperature ($\sim$5000 K) exceeds that of any containment vessel, and since the solid sublimes at low ambient pressure, long-term confinement at elevated temperature and pressure is impossible. Consequently experiments must rely on transient melting and probing, using methods such as shock waves,[15] pulsed ohmic heating[4] in high pressure cells,[14] and pulsed laser heating.[3,5,8–13]

Recent pulsed laser melting experiments[5,8,12,13] were the focus of a particularly sharp disagreement because of the apparent contradiction in measured properties. On the one hand, 30-ns laser pulses incident on highly oriented pyrolytic graphite (HOPG) created melt depths which Steinbeck *et al.*[5] could explain only by assuming large, metallic thermal conductivities in the melt. This result agreed qualitatively with metallic electrical resistivity ($\rho\sim 50\pm 20$ $\mu\Omega$ cm) measured by microsecond pulsed ohmic heating of pyrolytic graphite fibers at low pressure.[4] On the other hand, in time-resolved optical reflectivity measurements of HOPG melted and probed by 20-ps laser pulses, Malvezzi *et al.*[8] observed *decreased* surface reflectivity following excitation above a critical melting fluence, which they interpreted as the formation of an insulating liquid phase. This interpretation was supported by an optoelectronic switching experiment[9] in which picosecond laser-melted HOPG functioned as the photoconductive gap material in a current transmission circuit, but challenged by authors[4] who argued that material ablation obscured the liquid surface within the 20 ps pulse duration, causing a reflectivity decrease unrelated to liquid carbon.

In an earlier Rapid Communication,[10] we briefly reported the first *femtosecond* time-resolved reflectivity experiments on HOPG. The current paper is a comprehensive report of these experiments, augmented with expanded data and analysis. Femtosecond time resolution provides the ultimate "inertial confinement" of a laser-melted sample, because there is no time in the first 1–2 ps, following femtosecond excitation for atoms to move away from the surface. Thus the optical integrity of the surface is preserved, and the question of hydrodynamic surface expansion, or ablation, does not arise during this time interval. At the same time, considerable evidence suggests that structural disordering, or melting, of the lattice[21,22] and equlibration of electron and lattice temperatures[23] progress substantially toward steady-state during this time interval. Thus a critical time window exists during which the optically smooth surface of a quasi-

steady-state liquid can be probed. Indeed the femtosecond experiments[10] showed sharply *increased* reflectivity for several picoseconds following excitation above the critical melting fluence, which decayed to the much lower values observed in ps experiments[8] only after time delays of 10 ps or more. This pattern closely matched the reflectivity response of the much better understood silicon when irradiated at several times the melting fluence by a femtosecond pulse, where it is generally attributed to ultrafast melting into a metallic liquid followed by the slower process of surface expansion.[21,22] Thus these earlier fs experiments defined the time scale during which the optical properties of the unobscured liquid should be measured following melting by a femtosecond pulse.

In this paper the measurement and analysis of the optical properties of femtosecond-laser-melted carbon during the initial increased reflectivity stage is carried out in much greater detail. Specifically, time-resolved reflectance data at a range of probe wavelengths ($700 > \lambda > 310$ nm), oblique incidence angles, and pump fluences is reported. Furthermore a dielectric function based on the Drude model is fit to the data. From the model, Drude parameters—conduction electron density and collision frequency—are extracted. There are three motivations for such detail. First, careful reflectance measurements have historically provided one of the most important experimental keys to the underlying electronic properties of liquid metals.[24] Second, the recent appearance of molecular dynamics simulations[6] and a density functional theory[7] of the liquid state of carbon provide testable predictions of optical properties which can be compared directly to our data. Third, the low-frequency limit of the optical dielectric function can be related to previous measurements[4,14] and calculations[6,7] of the dc electrical resistivity of liquid carbon. Our results show much higher resistivity ($\rho \sim 600$ $\mu\Omega$ cm) than ohmically heated carbon at low pressure[4] or liquid silicon and germanium,[25] but agree closely with measured resistivity ($\rho \sim 1000$ $\mu\Omega$ cm) of carbon melted by ohmic heating at high pressure.[14] Additional new points of the current paper are time-resolved reflectance data of femtosecond-laser-melted diamond, which closely corroborate the graphite results, an analysis of the morphology of the damage spot produced above the critical melting fluence and its relationship to ablation, and a quantitative model of the delayed reflectivity decrease as a surface hydrodynamic expansion.

The paper is organized as follows. Section II discussed experimental methods. Section III presents experimental results of three kinds: (a) postmortem analysis of sample damage morphology, (b) self-reflectivity and -transmission of 90-fs pulses, and (c) pump-and-probe reflectivity and transmission measurements of HOPG and diamond at several probe wavelengths and polarizations. Section IV discusses the thermodynamic conditions which exist in the first picoseconds after intense femtosecond excitation: the rate of hydrodynamic surface expansion, the estimated extent of electronic and structural equilibration in the melt prior to surface expansion, and the estimated magnitude and time evolution of the transient temperature and pressure. Finally in Sec. V, we analyze the optical properties of liquid carbon by applying a Drude model to femtosecond reflectance measurements at $\Delta t \sim 1$ ps, after excitation, and relate this analysis to other measurements[4,14] and theories[6,7] of the liquid state of carbon.

II. EXPERIMENTAL METHODS

Experiments were performed with samples of highly oriented pyrolytic graphite (HOPG) and 250 μm thick, type IIa (100) diamond obtained from Dubbledee Diamond Corporation. The basic material properties of both the HOPG and diamond are described in detail elsewhere.[5,26,27] Throughout this work, many of the measurements were repeated under identical conditions on a reference silicon sample, which, because of its structural similarity and extensive previous studies of its femtosecond melting dynamics[21,22,28] and equilibrium liquid state (see Ref. 43), served both as a calibration and an aid in interpreting results. All measurements were made in air. The surfaces of the HOPG samples (normal to the graphite c axis) were prepared by using tape to peel off the first few layers immediately before each set of measurements to expose a fresh surface. The diamond surfaces were prepared by standard optical polishing techniques. Laser pulses of 90 fs duration, centered at 620 nm, and up to 0.2 mJ energy were provided by a colliding pulse mode-locked (CPM) ring dye laser[29] followed by a four stage Nd:YAG pumped optical dye amplifier system[30] operating at a 10-Hz repetition rate.

When freshly prepared surfaces were excited by a 90-fs, 620-nm pulse above a critical fluence F_m, a damage spot appeared. The fluence of incident pump pulses was calibrated by measuring their energy with a calibrated photodiode, while measuring the focused spot size at the sample surface by monitoring transmission through a pinhole (mounted in the same plane as the sample) translated across the focal spot. At each of several fluences thus calibrated, a sampling of irradiated spots was examined under Nomarski and scanning electron microscopes, and F_m was defined as the minimum fluence at which any change in surface morphology attributable to the laser pulse (e.g., amorphization, cratering) was observed.[31] Measured values of F_m are reported and discussed in the next section. F_m of a reference silicon wafer, measured by the same procedure, agreed with the value 0.1 J/cm^2 reported by other investigators for 90-fs, 620-nm pulses.[21,22,29]

At fluences $F > F_m$, the diameter and depth of the craters created by irradiation pulses was measured as a function of fluence in HOPG, diamond, and the reference silicon sample. The average radius of the damage spot r_{dam} at each fluence for a common focal spot size was determined by examining a statistical sampling of damage spots under a Nomarski microscope. Damage crater profiles were mapped with approximately 30-Å resolution using an Alpha-Step depth profiler. These depth profiles help in estimating the amount of material removed from the surface, and thus in evaluating the role of ablation in the experiments.

Two types of surface reflectance measurements were

performed: (1) self-reflectance of single 90-fs, 620-nm, near-normally incident pulses as a function of fluence, and (2) pump-probe measurements using a 90-fs, 620-nm, normally incident pump pulse and 90-fs probe pulses of varying wavelength ($310 < \lambda_{probe} < 700$ nm), polarization, and incidence angle. In addition, with diamond, transmission measurements were performed. Self-reflectivity measurements were performed on HOPG by focusing pulses to 50-μm diameter at a 10° angle of incidence onto the sample surface, collecting and imaging[21] the reflected pulses, then detecting only the center of the pulse profile, which was selectivity apertured in the image plane. This procedure avoided spatial averaging over a transverse fluence distribution. Thirty shots were taken at each fluence, and a matched reference photodiode monitored the pulse energy incident on the sample to provide normalization against shot-to-shot energy fluctuations, permitting reliable measurement of reflectance changes smaller than 1%. The sample was translated 150 μm after each laser shot to ensure that each shot interrogated a fresh region of the surface. A computer controlled the acquisition and shot-to-shot subtraction of the signal and reference voltages and the movement of the sample raster stage. The onset of surface morphology changes provided in situ calibration of absolute laser fluence.

Pump-and-probe measurements monitored the temporal evolution of reflectivity changes induced by surface melting. For these experiments, a beamsplitter divided the amplified pulses into pump and probe pulses. The pump beam was sent through a computer controlled optical delay line and focused to a spot diameter of 60 μm (HOPG) or 30 μm (diamond) at normal incidence onto the sample surface. The probe beam was attenuated to well below F_m. Time-resolved reflectivity and transmission of diamond was probed only at near normal incidence with 620-nm pulses, because of the limited amount of sample available. Normal incidence reflectivity of HOPG was probed not only at 620 nm, but at different wavelengths generated either by frequency doubling in a thin, phase matched potassium dihydrogen phosphate (KDP) crystal (to produce 310-nm pulses) or by white light continuum[32] in a jet of ethylene glycol (to generate pulses at $700 < \lambda < 500$ nm). Band-pass filters selected the appropriate wavelength for detection. In addition reflectance was probed at an oblique incidence angle ($\theta = 50°$) with s and p polarizations. Steeper incidence angles, though valuable for characterizing the dielectric function precisely,[25] were avoided because of the much greater difficulty of fully overlapping the pump and probe spots on the sample, and thus in obtaining quantitatively accurate absolute reflectance values. The probe beam was focused to a spot diameter of approximately 30 μm (HOPG) or 15 μm (diamond) in the center of the pump spot. Acquisition and shot-to-shot normalization were accomplished as described above. As an additional normalization, each spot was probed twice: first without, then with the pump, accomplished by blocking, then transmitting alternate pump pulses with an electronically controlled shutter. The difference between these two signals, each separately normalized to the reference photodiode signal, measured the change in reflectivity (HOPG, diamond) and transmission (diamond). Multiple laser shots at each time delay were then averaged. This procedure corrected for possible surface nonuniformities as the sample was rastered, and significantly improved signal-to-noise ratio, reproducibility, and accuracy of the measured *absolute* values of surface reflectivity. With the reference silicon sample, this procedure yielded absolute reflectance within 5% of independently measured values (see Ref. 43).[21,22,25] Such measurement accuracy is critical to extraction of accurate Drude parameters, and thus to conclusions regarding the nature of the liquid state of carbon. The temporal zero-delay (t_0) between pump and probe was calibrated to within ± 15 fs by monitoring the well-characterized reflectivity response[21,22,28] of the melting transition of the reference silicon sample.

III. EXPERIMENTAL RESULTS AND ANALYSIS

A. Postmortem analysis of sample damage

Using the procedure described above, we find the critical damage fluence F_m of HOPG to be 0.13 ± 0.02 J/cm^2 for single 620-nm, 90-fs optical pulses, very close to the value of 0.14 J/cm^2 determined by Malvezzi *et al.*[8] using 20-ps, 532-nm pulses. From known equilibrium material properties of HOPG,[5,26] we can calculate the final, equilibrated surface temperature T_f reached slightly below F_m (independent of the dynamical pathway by which it is reached) by equating absorbed optical energy to the integrated heat capacity:

$$(1-R)F_m\alpha = \rho \int_{300\ \mathrm{K}}^{T_f} C_p(T)dT \ . \tag{1}$$

We assume temperature-independent density $\rho = 2.25$ g/cm^3 and linear absorption ($\alpha^{-1} = 300$ Å), which is nearly the same for 620 and 532 nm.[26] A functional form of temperature-dependent heat capacity $C_p(T)$ below the melting temperature is given by Eq. (9) of Ref. 5, and pump pulse reflectivity $R \sim 0.3$ at F_m has been measured directly (see next section). The time constant for vertical heat diffusion out of the absorption volume is approximately 500 ps,[23,26] and can be neglected on the time scale (~ 1 ps)[23] on which an equilibrium temperature is established. We obtain $T_f \sim 6000$ K for both 20-ps and 90-fs pulses, 20–50% higher than the high pressure melting temperature,[2] of HOPG. However, the actual temperature is somewhat lower because the interband absorption saturates[23] as fluence approaches F_m, reducing the value of α by 30–50% in Eq. (1). This simple equilibrium analysis shows the HOPG indeed reaches the melting temperature at F_m, and suggests that melting occurs and causes the damage spot to form at $F > F_m$.

The damage threshold for diamond was measured to be 0.63 ± 0.15 J/cm^2 for 620-nm, 90-fs pulses. The fivefold higher value can be attributed to the requirement for simultaneous absorption of at least three 2.0-eV photons to cross the indirect energy gap E_g of 5.48 eV in diamond.[27] Self-reflectivity and transmission measurements presented below indeed confirm that strongly nonlinear absorption is present at fluences just below F_m, although

the final surface temperature T_f is therefore difficult to compute accurately because α depends strongly on the pulse energy and intensity profile.

Figure 1 presents measurements of the average damage spot radius as a function of the fluence of a normally incident 90-fs pump pulse focused to a spot radius of 30 μm on HOPG, or 15 μm on diamond. At F_m, a small damage spot (only a few microns in radius) appears in the center of the irradiated area. For $F > F_m$, the damage radius increases, at first rapidly, then more slowly with increasing fluence. For thermal melting by a pulse with Gaussian spatial profile $F = F_0 \exp(-r^2/\rho_0^2)$, the damage spot radius should increase with fluence as[33] $r_{\text{dam}} = \rho_0[\ln(F_0/F_m)]^{1/2}$, which is the fraction of the pulse cross-sectional profile in which $F > F_m$. The curves through the data points in Fig. 1 are fits of this formula to the measured damage radii using $\rho_0 = 30$ μm (HOPG) or 15 μm (diamond), which agree with the independently measured pump spot radius. From Fig. 1 we can determine that for $F > 0.4$ J/cm^2 (HOPG) or 1.5 J/cm^2 (diamond), the damage spot encloses $> 95\%$ of the energy of a Gaussian profile probe pulse focused as described above. However, below this fluence, any fluence dependence to the probe reflectivity must be attributed partly to the changing size of the melted region.

Figures 2(a) and 2(b) present measured depth profiles across the center of representative damage spots induced by 90-fs, 620-nm pulses in HOPG and silicon, respectively. Profiles of regions irradiated below F_m show no evidence of craters in either material. At 2.0 F_m (0.26 J/cm^2) in HOPG, a typical crater with a depth of ~ 300 Å is shown. In silicon, although amorphization, a signature of prior melting and rapid recrystallization, is clearly seen under a microscope in the irradiated region,[33] the depth profile still shows insignificant cratering at 2.0 F_m (0.2 J/cm^2). At 4.0 F_m, a typically deeper and wider crater is shown for HOPG, whereas the crater shown for silicon at 5.0 F_m is still small by comparison. The plot of average crater depth versus fluence (normalized to F_m) in Fig. 2(c) summarizes measurements of numerous damage spots in HOPG (filled squares) and silicon (open squares). For HOPG, *measurable craters are observed at all fluences above the damage threshold,* indicating that material has been lifted off the surface. The depths increase monotonically with increasing fluence, approaching 1000 Å at 12 F_m. In silicon, on the other hand, measurable craters are observed only for $F > 2.5F_m$, and increase in depth up to about $6F_m$. At fluences above about $10F_m$ in silicon, surface mounds appear, which may be caused by freezing of the molten silicon after being subjected to hydrodynamic shock from the laser pulse.[31] The higher threshold for crater formation in silicon can be attributed quantitatively[21] to the additional energy required to heat the stable liquid to the vaporization temperature, and to provide the latent heat of vaporization. Thus for $F > 2.5F_m$, the liquid is above the vaporization temperature. Most carbon phase diagrams,[2] on the other hand, show that the liquid phase exists in equilibrium only at pressures above 100 atm, and is thus thermodynamically unstable at atmospheric pressure, where it tends to sublime. Consequently, material loss to vaporization is expected as soon as the liquid phase is formed at F_m. With femtosecond excitation at $F > F_m$, material loss is probably enhanced compared to longer pulsed excitation, because of the initially elevated pressure (see Sec. IV).

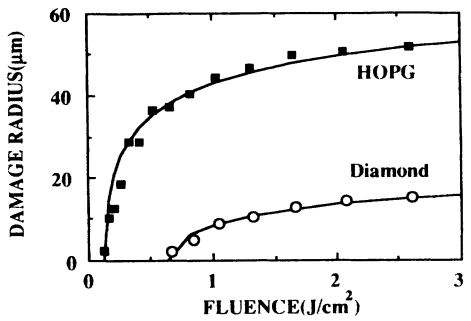

FIG. 1. Average radius of damaged area as a function of pump fluence for HOPG (solid squares) and diamond (open squares) after photoexcitation by 90-fs, 620-nm laser pulses focused to $1/e$ spot radius of 30 μm (HOPG) or 7.5 μm (diamond).

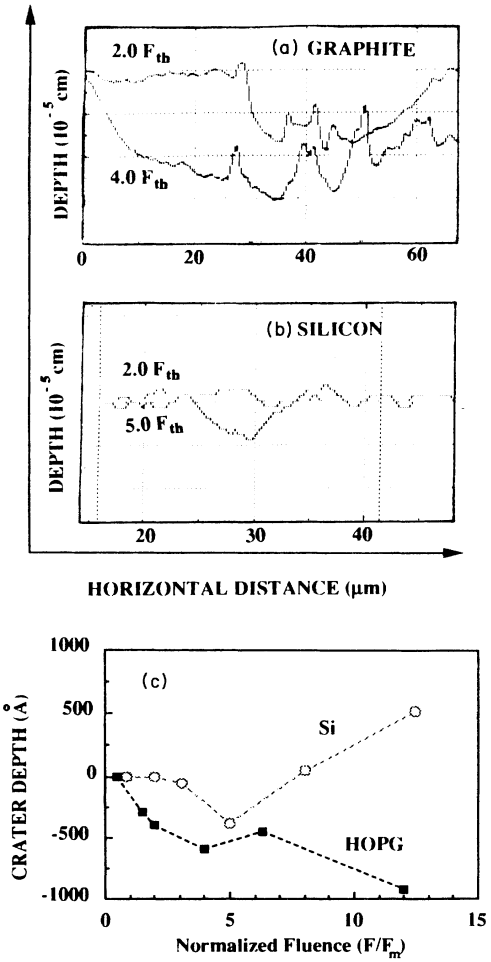

FIG. 2. Depth profiles of representative damage craters on (a) HOPG and (b) silicon for two fluences F above the critical melting fluence F_m. (c) Average crater depth as a function of F/F_m for HOPG (solid squares) and silicon (open squares).

B. Self-reflectivity and transmission

1. Graphite

Figure 3(a) shows the near-normal incidence self-reflectivity of the central part of the profile of 620-nm, 90-fs pulses from HOPG as a function of fluence normalized to F_m. Below F_m, the measured self-reflectivity is fluence independent and indistinguishable from the value of 0.3 measured for unexcited HOPG. Precisely at F_m, however, self-reflectivity begins to rise, reaching a values above 0.5 at $2OF_m$. This result contrasts with the self-reflectivity response observed by Malvezzi *et al.*[8] using 532-nm, 20-ps pulses, where self-reflectivity *decreases* above F_m.

2. Diamond

Figure 3(b) shows the self-reflectivity (R) and self-transmission (T) of near-normally incident 620-nm, 90-fs pulses in diamond as a function of normalized fluence. In this case the entire reflected and transmitted pulse energies were monitored, and the plotted R and T values include the fraction of pulse energy which was multiply reflected between the faces of the 250-μm-thick sample. At very low fluences ($F<0.01F_m$), $R+T=1$, signifying the absence of absorption. In the range $0.01F_m<F<F_m$, R remains nearly fluence independent, while T drops sharply to less than $\frac{1}{3}$ of its low fluence value, a clear signature of multiphoton absorption. A fit of the data to a three-photon absorption model[11] yields a three-photon absorption coefficient $\gamma\sim 25$ cm$^3/TW^2$, although the data is not sufficiently accurate to rule out the simultaneous presence of higher order absorption nonlineraities. Precisely at F_m, self-reflectivity begins to increase sharply, just as observed in HOPG, while self-transmission continues to decrease.

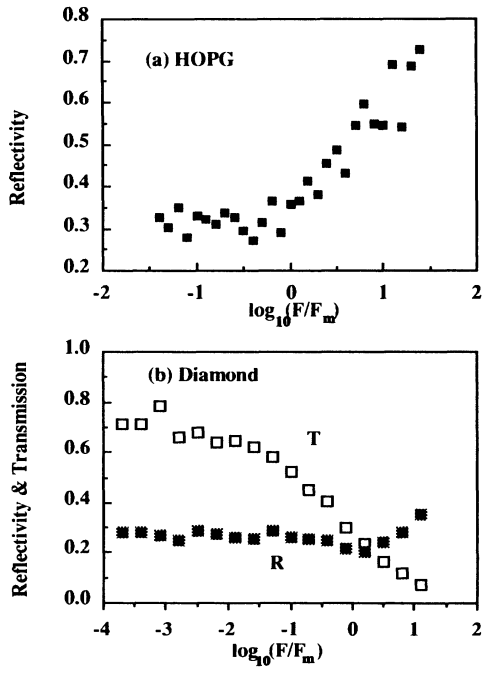

FIG. 3. (a) Self-reflectivity of 90-fs, 620-nm pulses normally incident on HOPG as a function of fluence F normalized to the critical melting fluence F_m. (b) Fluence dependent self-reflectivity and transmission of 90-fs, 620-nm pulses normally incident on diamond.

The *precise* correlation between the self-reflectivity increase and the damage threshold in both samples suggests that the increase is caused by the initial dynamics of the melting process which occur during the pump pulse, as discussed further in Sec. IV. Measurements of the related process of *two*-photon absorption of 4.0-eV femtosecond pulses in diamond have been presented elsewhere.[34]

C. Femtosecond pump-probe measurements

1. Graphite

a. 620-nm wavelength probe, the first 25 ps. Figure 4 presents the time-resolved reflectivity of 620-nm probe pulses from HOPG for the first 25 ps following excitation above F_m as the pump fluence increases from 0.5 J/cm^2 to 20 J/cm^2. This time interval is long enough to show all of the major features of the reflectivity response with relatively coarse time resolution. Beyond $\Delta t=25$ ps, the visible reflectivity remains nearly constant for approximately a nanosecond, as also observed by Malvezzi *et al.*[8]

Figure 4(a) shows three reflectivity responses corresponding to a common pump fluence ($F=0.5$ J/cm^2), but to three different probe polarizations: s polarized at $\theta=50°$, near normal incidence, and p polarized at $\theta=50°$. The measured reflectivities for $\Delta t<0$ agree with Fresnel equation predictions when the published optical constants[26] $n=2.6$, $k=1.5$ for unexcited graphite at 620 nm are used. For $\Delta t\geq 0$, the inequality $R_s(\theta=50°)>R_p(\theta=10°)>R_p(\theta=50°)$ is maintained at all time delays. At $\Delta t=0$, reflectivity increases sharply with a pulse width limited rise time to a value roughly 50% higher than the initial value. There is a slight "overshoot" in the reflectivity, evident as only a single data point on this coarse time scale, which recovers in a fraction of a picosecond. There follows a slower decay to the initial value in ~ 8 ps, then a continuing drop to a final steady state value in 20 to 40 ps. From the three measured reflectivities, the complex index of refraction $n+ik$ can be determined uniquely at any time delay from Fresnel's equations, provided that the surface is assumed to remain perfectly discrete. Thus at 0.3 ps$<\Delta t<1$ ps, we obtain $n=1.35$, $k=1.93$, showing increased metallic character. At time delays greater than several picoseconds, however, the assumption of a discrete interface may no longer be valid, as discussed further in Sec. IV.

Figures 4(b) and 4(c) show the reflectivity response probed at near normal incidence at progressively higher pump fluences of 2.0 and 3.9 J/cm^2, respectively. Again reflectivity increases sharply at $\Delta t=0$, reaching a maximum value which increases slightly with pump fluence. The subsequent drop in reflectivity depends strongly on pump fluence. The reflectivity decays more rapidly, and

the final reflectivity value becomes smaller, as pump fluence increases. This trend continues at higher fluences, as shown by the oblique incidence probe reflectivity data at 20 J/cm^2 pump fluence in Fig. 4(d) (data for a near normally incident probe is not shown in this figure). The general pattern of a sharp reflectivity increase followed by a slower, but fluence-dependent decrease closely resembles the reflectivity response of silicon[21,28] when melted by femtosecond pulses above the vaporization fluence $F > 2.5F_m \sim 0.25$ J/cm^2. The main difference is that in silicon the reflectivity decay is not observed for pump fluences $F_m < F < 2.5F_m$ between the melting and vaporization fluences, whereas in HOPG, the decay is observed at all fluences $F > F_m$. Thus the reflectivity decay correlates with the appearance of damage craters described above, suggesting that hydrodynamic surface expansion causes the reflectivity decay.

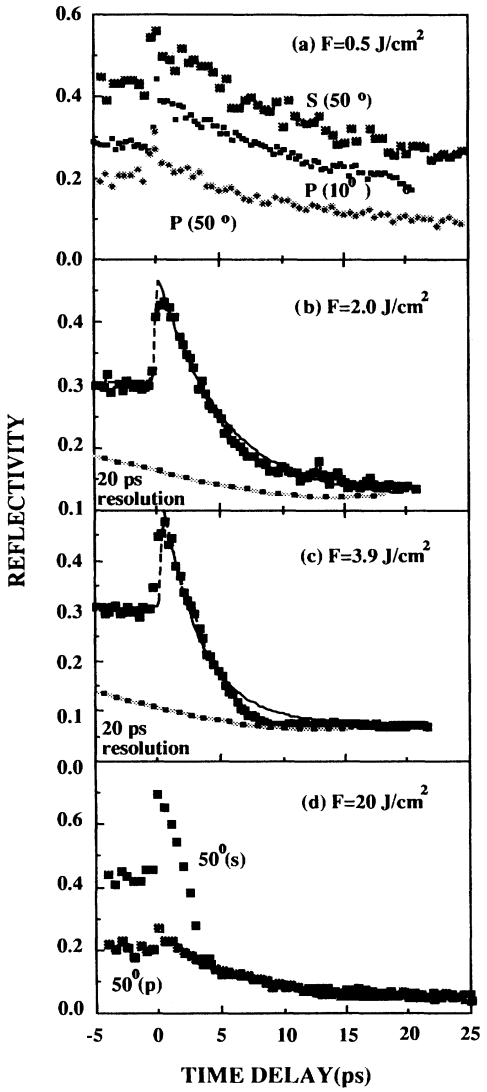

FIG. 4. Femtosecond time-resolved reflectivity of HOPG. (a) Excitation at pump fluence $F = 0.5$ J/cm^2, probe at 620 nm, comparing 50° incident angle s and p polarized reflectivity, and near-normal incidence reflectivity. (b) Near-normal incidence 620-nm reflectivity at $F = 2.0$ J/cm^2; dashed line shows convolution of data with 20-ps pump and probe pulses. (c) Same with $F = 3.9$ J/cm^2. (d) Excitation at 20 J/cm^2, probe at 620 nm, comparing 50° incident angle s and p polarized reflectivity. Vertical scales on all panels denote absolute reflectivity.

It is helpful to fit the observed reflectivity responses in Figs. 4(a)–4(d) phenomenologically to a function $R(\Delta t)$, which convolves a single exponential response function $r(t) = \exp[-(t-t')/\tau_a] - C$ with the temporal intensity envelopes $P_{\text{pump}}(t)$ and $P_{\text{probe}}(t)$ of the pump and the probe pulses:

$$R(\Delta t) = \int_{-\infty}^{\infty} P_{\text{probe}}(t+\Delta t) \int_{-\infty}^{t} P_{\text{pump}}(t') r(t') dt' dt \ . \tag{2}$$

τ_a is the relaxation time constant, and the modified baseline C represents the final reflectivity value. The pump and probe intensity envelopes are conveniently represented as $\text{sech}^2(t/\tau_p)$. Examples of fits to Eq. (2), using the measured pulse width $\tau_p = 90$ fs, are shown by the curves superimposed on the data in Figs. 4(b) and 4(c) where time constants $\tau_a = 6$ and 4 ps, respectively, were used. Fits of equal quality are obtained for other fluences. In Fig. 5 these decay time constants obtained in the same manner from femtosecond reflectivity data on silicon photoexcited at $F > 0.25$ J/cm^2 are also plotted (solid circles). For similar fluences, similar time constants are obtained in HOPG and silicon. The solid line is a theoretical curve which predicts a characteristic time constant for hydrodynamic surface expansion, which decreases with laser fluence in a manner very similar to τ_a. This model is discussed further in Sec. IV.

Equation (2) can also be used to calculate the reflectivity response $R(\Delta t)$ which would be observed in an experiment with longer pump and probe pulses. The grey-tone curves in Figs. 4(b) and 4(c) were obtained using the same response function $r(t)$, but $\tau_p = 20$ ps, corresponding to the pulse duration used by Malvezzi *et al.*[8] Clearly the initial reflectivity increase cannot be observed at all with this time resolution. In addition, the fluence dependence of the reflectivity drop is largely masked. Consequently the calculated response shows only a

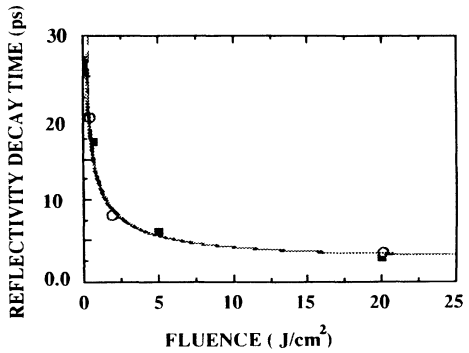

FIG. 5. Fluence dependence of the decay time constant of the reflectivity response of HOPG (open circles) and silicon (solid circles). The solid line is a theoretical fit to a $F^{-1/2}$ dependence, as discussed in the text.

monotonic reflectivity drop following photoexcitation, consistent with the picosecond data of Malvezzi *et al.*[8]

One additional feature of the Fig. 4 data is noteworthy. Maximum *s*-polarized reflectivity, observed at $\Delta t \sim 1$ ps, increases form 0.58 at 0.5 J/cm^2 [Fig. 4(a)] to 0.69 at 20 J/cm^2 [Fig. 4(d)], a trend also observed in normal incidence reflectivity. Maximum *p*-polarized reflectivity, on the other hand, *decreases* from 0.3 (0.5 J/cm^2) to 0.26 (20 J/cm^2). The selective suppression of *p*-polarized reflectivity at such a high fluence as 20 J/cm^2 probably results from a significant degree of ionization, and the formation of a short scale length plasma density gradient at the surface. Consequently resonance absorption selectively attenuates *p*-polarized light.[35] Similar effects have been observed and analyzed by Milchberg *et al.*[36] Since *s*- and *p*-polarized reflectivity increase about equally at lower fluences [e.g., Fig. 4(a)], however, we can assume that the surface is discrete at early time delays.

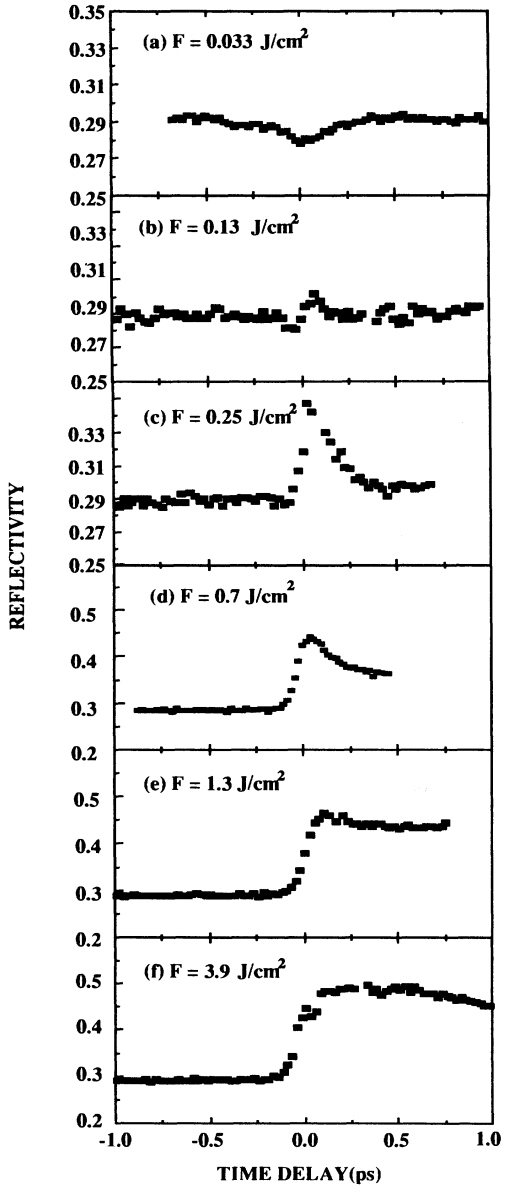

FIG. 6. The first picosecond of the time-resolved reflectivity response of HOPG probed by 90-fs, 620-nm pulses at near normal incidence. (a) Excitation at pump fluence F below critical melting fluence F_m; (b) $F = F_m$; (c)–(f) increasing fluences above F_m. Vertical scales denote absolute reflectivity.

b. 620-nm probe wavelength, the first picosecond. Fine time-scale data over the first picosecond documents the initial stage of photoexcitation and melting dynamics. Figure 6 shows the first picosecond of the reflectivity response probed at near-normal incidence as the pump fluence is varied from 0.033 to 3.9 J/cm^2. Just below the threshold [$F = 0.033$ J/cm^2, Fig. 2(a)], a small decrease in reflectivity is observed during the pump pulse, which recovers in $\sim$200 fs. This response is caused by the generation, relaxation, and recombination of an electron-hole plasma, and is in good quantitative agreement with the extensive reflectivity measurements below F_m reported by Seibert *et al.*[23] When the pump fluence is increased to exactly 0.13 J/cm^2, a nearly flat response is seen, as shown in Fig. 2(b). As soon as the fluence is increased above F_m, a sharp reflectivity *increase* is observed [$F = 0.25$ J/cm^2, Fig. 2(c)], followed by a fast ($\sim$200 fs) recovery and a small residual reflectivity increase, which persists for over 10 ps. For the data in Figs. 2(b) and 2(c), the damage spots were smaller than the probe spot. Consequently, the measured response averages the actual response below and above F_m to some extent. At higher fluences, however, essentially the entire probe pulse sees material excited above F_m. At $F = 0.7$ J/cm^2 and 1.3 J/cm^2 [Figs. 2(d) and 2(e)], the fast transient is still evident, but the persistent reflectivity component increases sharply in magnitude to over 0.4. At still higher pump fluence [$F = 3.9$ J/cm^2, Fig. 2(f)], the fast transient is no longer evident, and a slight further increase to $R \sim 0.5$ occurs.

Two important features of the initial reflectivity response above F_m are noteworthy. First, the rise times of reflectivity signals in Figs. 6(c)–6(e) are all pulse width limited. This contrasts with a resolvable delay of $\sim$200 fs in the rise time of the reflectivity of silicon when photoexcited just above F_m.[22] This comparison suggests that the initial response of HOPG above F_m is caused by an overdense electron-hole plasma, which rapidly equilibrates, whereas the electron-hole plasma in silicon fails to reach critical density just above F_m, yielding a response time governed by the melting dynamics. Second, the fast transient observed above F_m, though opposite in sign, recovers on the same time scale as the transient observed below F_m [Fig. 6(a) and Ref. 23]. This comparison suggests that the former, like the latter,[23] is also caused by equilibration of hot electrons with the lattice, as discussed further in Sec. IV.

c. Other probe wavelengths. A reflectivity spectrum over as wide a range of wavelengths as possible is key to modeling the underlying electronic structure of liquid carbon. Figure 7 shows the time-resolved reflectivity of 310-nm, probe pulses from HOPG following excitation below F_m [Fig. 7(a)] and at two fluences above F_m [Figs. 7(b) and 7(c)]. The response differs substantially from that at 620 nm. Following sample excitation at $0.1F_m$

[Fig. 7(a)], ultraviolet reflectivity first decreases for the first 100 fs, then recovers within 2 ps to a steady-state value 4% higher that the initial reflectivity, which persists for ~500 ps. A detailed interpretation of this response has been presented elsewhere.[23] The initial decrease is caused by the rapid generation and energy relaxation of electrons and holes, while the slowly rising reflectivity is caused by the thermal renormalization of the graphite π energy bands,[23] and provides a measure of the time required for full electron-lattice equilibration. The ultraviolet reflectivity response above F_m differs significantly from the response when excited below F_m, providing further evidence that an irreversible phase transition occurs at F_m. At $F=0.7$ J/cm^2, no reflectivity increase whatsoever is observed with the ultraviolet probe, in sharp contrast to the 620-nm, probe [Figs. 4(a) and 6(d)]. Instead, reflectivity remains unchanged for the first picosecond, then monotonically decreases within 20 ps to a steady-state value ($R=0.05$), which persists for at least 300 ps. When pump fluence is increased, the reflectivity drops more rapidly, and to a lower final value, the same trends observed with the 620-nm, probe. In addition, when the pump fluence is increased to 4 J/cm^2, a slight transient reflectivity increase (barely above the noise level) is observed during the first ~0.5 ps, as shown on the magnified scale of Fig. 7(b). This transient evolves on approximately the same time scale as the reflectivity transients shown in Figs. 6(a)–6(e) and 7(a). We attribute this to the initially nonequilibrium electron-hole plasma which at this fluence has become sufficiently dense to be detected at 310 nm.

Figure 8 shows fluence dependent reflectivity measurements made at fixed time delays of 0.7 and 20 ps, using a white light continuum probe, where wavelengths of 550 nm [Fig. 8(a)], 620 nm [Fig. 8(b)], and 700 nm [Fig. 8(c)] were selected for detection. A delay of 0.7 ps probes the high reflectivity portion of the evolution after the initial transient 200-fs features, while a delay of 20 ps probes the approach to a low steady-state reflectivity. In both cases, no change in reflectivity occurs until the critical melting threshold is reached. At $\Delta t=0.7$ ps, the reflectivity begins to rise precisely at the critical melting fluence at *all* probe wavelengths, reaching a final value of $\sim 1.5R_0$ at $10F_m$. In addition, the reflectivity scales equally with

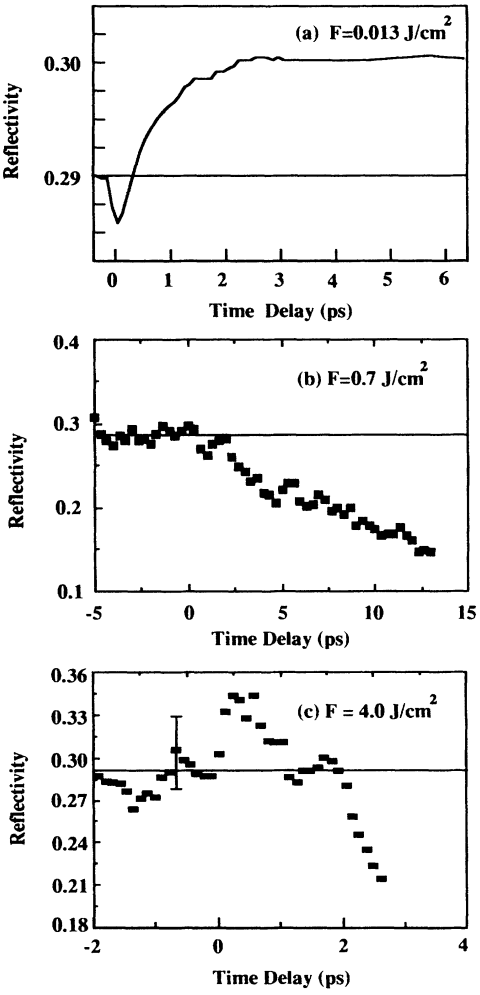

FIG. 7. Time-resolved reflectivity response of HOPG probed by 90-fs, 310-nm pulses at near normal incidence for three fluences F of the 90-fs, 620-nm pump pulse: (a) $F=0.1F_m$, (b) $F=5F_m$, (c) $F=30F_m$.

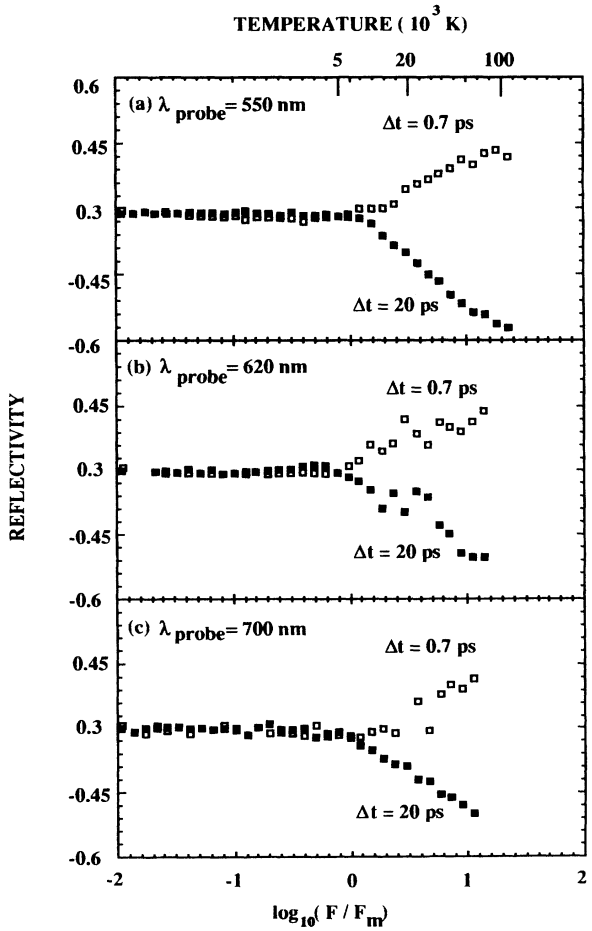

FIG. 8. Reflectivity of HOPG as a function of normalized pump fluence F/F_m for probe delays of 0.7 and 20 ps, for probe wavelengths (a) 550 nm, (b) 620 nm, (c) 700 nm.

fluence in each case. Spot size effects contribute to the increasing magnitude of the reflectivity in the fluence range $F_m < F < 3F_m$. Above $3F_m$, however, the increasing reflectivity is caused entirely by changing properties of the material as its temperature increases. The scale at the top of Fig. 8(a) gives a rough estimate (±50%) of sample temperature at $\Delta t = 0.7$ ps derived by an extension of Eq. (1), as discussed further in Sec. IV. At a given fluence (temperature) reflectivity is slightly higher at longer wavelengths. At $\Delta t = 20$ ps, for all wavelengths, the reflectivity drops below the background HOPG value precisely at the critical melting fluence, and decreases monotonically with fluence. A very slight rise in reflectivity is observed below the critical melting fluence at 620 nm, as observed in previous studies[23] below F_m, and is related to electron-hole carrier generation.

2. Diamond

Below F_m very different femtosecond responses are expected in graphite and diamond, because of the very different electronic band structures. Above F_m, however, we expect to measure similar optical properties, if the two samples melt and equilibrate to a common liquid phase on the time scale of the measurements.

Figure 9 shows the time-resolved reflectivity and transmission of 620-nm probe pulses from diamond following excitation just below F_m [Fig. 9(a)] and well above F_m [Figs. 9(b) and 9(c)]. For these measurements, the probe is incident at a large enough angle ($\sim 20°$) that the front surface reflection has been spatially separated from the back surface reflection. Below F_m [Fig. 9(a)], no change in front surface reflectivity was detectable. However, transmission drops to 0.45 immediately upon photoexcitation, with negligible recovery over tens of picoseconds. We believe this response to be free carrier absorption in an electron-hole plasma generated by three-photon absorption. The recovery rate is severely limited compared to graphite because of the large energy gap which separates electrons and holes following their relaxation to band edges. Above F_m, we observe on a coarse time scale [Fig. 9(c)] a reflectivity response qualitatively very similar to the graphite responses shown in Figs. 4: a sharp initial increase followed by a slower decay over ~ 10 ps. The lower peak reflectivity value (~ 0.3) compared to HOPG excited at $10F_m$ (~ 0.45) is partly an artifact resulting from the coarse time spacing of data points used to conserve sample area in taking the Fig. 9(c) data. When repeated at the same fluence ($F = 9F_m$) with finer time resolution over a shorter time interval [Fig. 9(c)], the data indeed show that diamond reflectivity increases from 0.17 to approximately 0.4, very close to, although still slightly lower than, the value observed with HOPG. This small discrepancy may be a real difference in the reflectivity of the liquid phases, perhaps because the liquid initially retains the higher density of diamond (3.5 g/cm^3) compared to graphite (2.2 g/cm^3).

The corresponding transmission response of diamond excited at $3F_m$ (solid squares) and $6F_m$ (open squares) is shown in Fig. 9(b). Transmission decreases abruptly at $\Delta t = 0$ from its unexcited value (0.7) to less than 0.2. On the time scale (25 ps) on which reflectivity undergoes large changes, no further change in transmission is observed. The slightly higher final transmission value at $3F_m$ results from the probe spot being slightly larger than the damage spot. A similar transmission response is observed with silicon-on-sapphire upon melting with a femtosecond pulse.

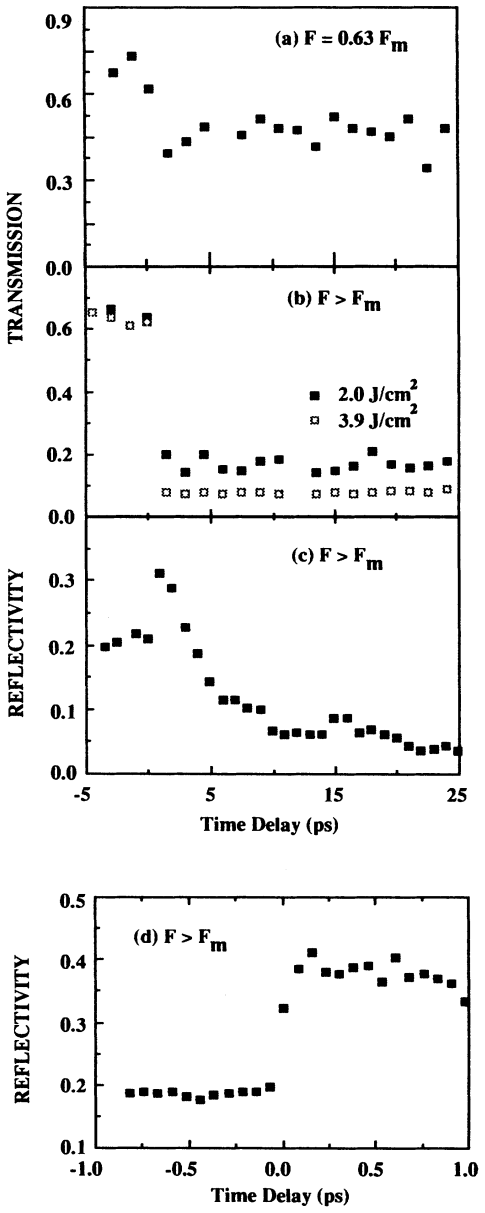

FIG. 9. Femtosecond time-resolved front surface reflectivity (R) and transmission (T) of diamond, probed at near normal incidence by 90-fs, 620-nm pulses. (a) Pump fluence $F = 0.6F_m$; (b) T at $F = 3F_m$ (solid squares) and $6F_m$ (open squares); (c) R at $F = 9F_m$ on coarse time scale; (d) detail of first picosecond of reflectivity response at $F = 9F_m$.

IV. DISCUSSION

A. Hydrodynamic surface expansion

In order to obtain meaningful optical data on the liquid phase, it is critical to collect data before surface optical properties deteriorate because of hydrodynamic expansion. Femtosecond experiments remove all ambiguity that the surface can be probed before the surface expands significantly. The consistent observation of an early reflectivity increase (unresolvable in ps experiments[8]) followed by a fluence dependent decrease is therefore simply and naturally explained as initial creation of a highly reflective condensed phase, which is subsequently obscured by surface expansion. Indeed there is general agreement[8,10,37] that at fluences $F > 5F_m$, ablation attenuates surface reflectivity within several picoseconds of photoexcitation.

Nevertheless, some authors[8,37] have argued that during a 20-ps melting pulse in the limited fluence range $F_m < F < 5F_m$, insufficient material can evaporate to affect surface reflectivity significantly, and that reduced reflectivity in this fluence range must therefore be ascribed to intrinsic (electrically insulating) properties of the condensed surface. Analogously, in our previous paper,[10] we did not rule out the possibility that the delayed reflectivity decrease for $F_m < F < 5F_m$ observed in fs experiments could be caused by a delayed metal-to-insulator transition within the liquid, which maintained a discrete, unobscured interface.

Several cogent arguments can now be advanced against this interpretation of the fs experiments. First, if the reflectivity decrease corresponded to an unobscured insulating material developing, a transmission recovery on the same time scale as the reflectivity decrease would be expected. Yet no such recovery is observed in the diamond transmission measurements at any pump fluence [Fig. 9(b)]. Instead transmission drops sharply upon photoexcitation to a value which remains constant for over 25 ps. On the other hand, this pattern is consistent with the early formation of a glossy, reflective liquid and subsequent surface expansion. Such transmission measurements were not available in the previous report on graphite.[10] Second, the careful damage morphology analysis now shows that delayed reflectivity decreases following fs melting in both graphite and silicon are *precisely correlated* with appearance of a damage crater, and thus with removal of material from the surface at some time after irradiation. Specifically, in silicon, damage craters and delayed reflectivity decreases[21] both are observed only for $F > 2.5F_m$, the fluence required to heat the liquid to the boiling temperature and provide the latent heat of vaporization; correspondingly in graphite, damage craters and a delayed reflectivity increase both occur for $F > F_m$, suggesting that liquid carbon spontaneously ablates at atmospheric pressure. Third, the time constants of the reflectivity decrease (Fig. 5), have nearly the same values and fluence dependence for femtosecond-irradiated carbon and silicon, suggesting a common ablative mechanism. Finally, no theoretical basis exists for structural or electronic equilibration within the liquid on a 10–30-ps time scale. On the contrary, recent molecular dynamics simulations of the liquid state of carbon[6] show that the liquid reaches steady state structural and electronic properties within ~ 1 ps of heating to the melting temperature.

In order to reconcile the observation of a strong reflectivity decrease within ~ 10 ps with the very small evaporation rate expected[8,37] at $F < 5F_m$, we must reconsider the microscopic mechanism for the reflectivity decrease. The "evaporation" model described in Refs. 8 and 37 in the context of ps irradiation depicts the escape of individual atoms from the liquid to form an absorptive vapor above the liquid surface, which is assumed to retain an atomically sharp interface. Indeed optical absorption from the expected vapor density at $\Delta t \sim 10$ ps is clearly inadequate to account for the observed reflectivity decrease at $F < 5F_m$. On the other hand, recent studies of metal surfaces irradiated by intense, femtosecond pulses[35,36] show that strong reflectivity decreases within a few picoseconds are caused by hydrodynamic expansion of the surface as a whole, because of the high transient pressure created by femtosecond irradiation (Sec. III C below). The initially atomically abrupt interface develops a short scale length density gradient shortly following excitation, similar to the hydrodynamic expansion of a surface experiencing a strong shock wave.[38] When the gradient scale length L approaches a significant fraction of an optical wavelength λ, surface reflectivity can no longer be described by Fresnel's equations, which are based on boundary conditions for an abrupt interface, but instead requires numerical treatment via the Helmholtz wave equation.[36] Typical calculations[35,36] show strong reflectivity decreases for $L > 0.2\lambda$, with complicated dependence on polarization, wavelength, material, and the precise form of the density gradient.

In order to estimate the time τ for such a density gradient to form under our experimental conditions, we use the expression for hydrodynamic expansion velocity of a surface experiencing a strong shock wave:[38]

$$\langle v \rangle = \frac{2}{\gamma - 1} \left[\frac{ZkT}{M} \right]^{1/2}, \tag{3}$$

where $\langle v \rangle$ is the average particle velocity in the normal direction, $\gamma = C_p / C_v$ is the ratio of electronic heat capacities at constant pressure and volume, Z is the effective ion charge, T is the surface (electron) temperature, and M is the mass of a carbon atom. Estimating $\gamma \sim 1.6$ and $Z \sim 4$ for carbon at high temperatures,[39] we obtain $\langle v \rangle \sim 2[k_B T(\text{eV})]^{1/2} \times 10^6$ cm/s, close to the speed of sound. To a fair approximation, $k_B T \sim 0.5$ eV at $F = F_m$, and $k_B T \propto F$ at higher fluences. Thus at $F = 4F_m$, for example, a scale length $L = 0.5\lambda = 310$ nm develops in a time $\tau = L / \langle v \rangle \sim 10$ ps, consistent with the time scale of the reflectivity decrease in Fig. 4(a). To obtain a fit to the fluence dependence of the exponential decay constants τ plotted in Fig. 5, we assume that surface reflectivity is reduced by e^{-1} when an L develops over a fraction $0.1 < f < 1$ of the probe wavelength λ, where f can be treated as a fitting parameter which depends on polarization, wavelength, material, and the form of the density

gradient. The time for the necessary gradient to form is then $\tau = f\lambda/\langle v \rangle$. As the fluence (and therefore T) increases, $\langle v \rangle$ increases as $(k_B T)^{1/2}$, resulting in a reduced gradient formation time. The solid (graphite) and dashed (silicon) theoretical curves in Fig. 5 are fits to the data obtained using $f = 0.6$ (graphite) or 0.15 (silicon), corresponding to $L = 3720$ Å (graphite) or 930 Å (silicon).

Thus both the magnitude and fluence dependence of the reflectivity decay time constant τ in both silicon and graphite (Fig. 5) are consistent with the one-dimensional expansion rate of condensed material surface into a vacuum after being pressurized and heated by the absorption of a femtosecond pump pulse. Significantly, the fluence dependence of τ for both $F_m < F < 5F_m$ and $F > 5F_m$ fit naturally to a *single model,* further confirming that the delayed reflectivity decreases in both fluence ranges of fs excitation are caused by a common mechanism of surface hydrodynamic expansion. Thus if the influence of hydrodynamic expansion is to be ruled out unambiguously, the optical properties of a condensed phase driven to elevated temperature and pressure by a femtosecond pulse must be probed within a critical time window of no more than a few picoseconds.

B. Electron-lattice and structural equilibration

A key question then becomes: to what extent has the photoexcited carbon equilibrated within the available time window? Several lines of evidence suggest that electron and lattice temperatures substantially equilibrate within ~ 1 ps following photoexcitation of the carbon sample. First, femtosecond spectroscopy of graphite excited *below* F_m shows[23] that photoexcited carriers relax almost completely within 1 ps. The graphite lattice temperature is measured directly by the rising UV reflectivity response in Fig. 7(a),[23] which confirms that, below F_m, the lattice reaches its maximum temperature within 2 ps, and has nearly reached the maximum within 1 ps. Similar or shorter electron-lattice equilibration times have been measured for many metals.[40] As the lattice melts, the increased disorder should further accelerate electron-lattice equilibration, as observed, for example, in comparisons of carrier lifetimes in crystalline,[41] amorphous,[42] and liquid[25] silicon.

Second, the subpicosecond reflectivity transient observed upon photoexciting graphite *above* F_m [Figs. 6(b)–6(e) and 7(c)] recovers on a similar time scale to the transient below F_m. In our previous paper,[10] we showed that this reflectivity "overshoot" at 620-nm, probe wavelength [Figs. 6(b)–6(e)] is explained by the instantaneous generation of an overdense electron-hole plasma ($N_{e\text{-}h} > 10^{22}$ cm^{-3}) upon photoexciting HOPG at $F \geq F_m$. With an ultraviolet probe [Figs. 7(b) and 7(c)], higher pump fluence ($\sim 10F_m$) and carrier density ($N_{e\text{-}h} > 4 \times 10^{22}$ cm^{-3}) is required to see this overshoot, as expected from the Drude dielectric function,[10] and confirms the interpretation of the overshoot as a short-lived electron hole plasma. The common subpicosecond recovery time of these reflectivity transients both below and above F_m supports the interpretation that electron and lattice subsystems equilibrate to nearly a common temperature within 1 ps.

Third, molecular dynamics (MD) simulation of the liquid state of carbon by Galli *et al.*[6] show that structural equilibration is also very rapid: the structural and electronic properties of an initial amorphous carbon structure heated to 5000 K in the electronic ground state reach a steady-state liquid structure in well under 1 ps. Simulations which begin by heating a crystalline graphite or diamond structure might yield a somewhat longer equilibration time, and would be of great interest in interpreting femtosecond experiments. Nevertheless our observation of very similar subpicosecond reflectivity evolution of graphite and diamond samples excited at $F > F_m$ [Figs. 6 and 9(c)] strongly suggests that both have equilibrated to a common liquid phase at $\Delta t \sim 1$ ps.

Finally, in a well-studied material as silicon, subpicosecond reflectivity transients are also observed,[28] but reach steady-state values within 1 ps[21,22] which are fully consistent with the independently measured optical properties of fully equilibrated, over-melted silicon.[25,43] In fact, femtosecond and picosecond experiments at $F_m < F < 2.5F_m$ show a constant reflectivity for 0.5 ps $< \Delta t <$ 1 ns or more.[21,25] Femtosecond surface second harmonic measurements[22] show that long-range crystalline order is lost in 0.5 ps, demonstrating that the measured reflectivity is indeed that of a liquid phase.

Available evidence thus supports the conclusion that optical properties probed at $\Delta t \sim 1$ ps are those of a liquid state of carbon with substantially equilibrated electron and lattice subsystems. At very high fluences $F \gg F_m$, the term "solid density plasma"[35,36] may be more appropriate than "liquid," in recognition of the higher ionization states[39] which accompany higher temperature and pressure conditions. However, there is no sharp demarcation between the two regimes, and both may be encompassed by the term "fluid."

C. Temperature and pressure following femtosecond excitation

For $F > F_m$, the quasiequilibrium temperature T_f of the liquid established by $\Delta t \sim 1$ ps can, in principle, be calculated by a generalization of Eq. (1) which takes into account variations in the absorption coefficient $\alpha(t)$ during the pump pulse, and the heat capacity $C_{\text{liquid}}(T)$ of the liquid phase. In practice, the variations in $\alpha(t)$ are quite complicated and $C_{\text{liquid}}(T)$ can only be estimated, thus precluding any more than a rough estimate of T_f of the liquid. The significant saturation (decrease in α) which occurs at fluences approaching F_m for HOPG has already been noted. On the other hand, above F_m, the onset of melting and metallic properties probably increases α later in the pump pulse. Thus as a compromise the linear absorption depth $\alpha^{-1} = 300$ Å of HOPG provides an approximate basis for estimating T_f. On the short time scale of $\Delta t \sim 1$ ps, volume expansion can be neglected ($\rho = \rho_0 = 2.25$ g/cm^3 for HOPG), and the heat capacity C_v at constant volume should be used. The specific heat $(3/2)Nk_B$ of a classical monatomic gas provides a basis for estimating for $C_{\text{liquid}}(T)$. Internal vibrational modes in the liquid would, of course, increase this value toward the Dulong-Petit value of $3Nk_B$. The mea-

sured pump self-reflectivities $R(F_m)$ in Fig. 3(a) can be used directly in Eq. (1). Combining these approximations, the temperature estimates on the upper horizontal axis of Fig. 8 were obtained, and indicate that temperatures as high as 100 000 K can be reached under our experimental conditions. The expected accuracy of this scale, however, is no better than ±50% in view of the above approximations.

When the sample is heated and probed on a time scale shorter than the characteristic time for thermal expansion, transient pressure exists because the sample is inertially confined to a constant volume. The magnitude of the pressure depends on the degree of equilibration within the phonon system. As an upper limit which assumes an equilibrated phonon system, the pressure p of a solid heated to $k_B T < 10$ eV (assuming $T_e = T_i = T$) at the constant density ρ_s of the low temperature solid is determined primarily by anharmonic ionic motion, and is described by the approximate formula $p \sim p_i \sim 3N\gamma k_B T$, where γ is the Gruneisen parameter.[44] More precisely, total pressure p also includes contributions from Thomas-Fermi electron pressure, and a correction for chemical bonding, but for $k_B T < 10$ eV and $\rho \sim \rho_s$, the ionic contribution p_i strongly dominates.[44] The dashed curves in Fig. 10 plot $p_{\text{ion}}(T)$ for liquid carbon for fixed densities corresponding to graphite (2.25 g/cm^3) or diamond (3.5 g/cm^3). The solid curves show $p(T)$ corrected for the electronic and bonding contributions [derived from Eqs. (81) and (106) of Ref. 44]. For completeness, the curves have been extended to $T < T_m$, using the corresponding expression for $\rho_{\text{ion}}(\rho, T)$ for a high temperature solid [Eq. 34(b) of Ref. 44]. Figure 10 shows that transient pressures of approximately 1 megabar can exist at $T > T_m$. The time scale τ_{rel} for release of the pressure is estimated from the ratio of the heated (absorption) depth α^{-1} to the speed of sound c_s. For HOPG, we estimate $\tau_{\text{rel}} \sim \alpha^{-1}/c_s \sim 5$ ps, using $\alpha^{-1} \sim 500$ Å and $c_s \sim 10^6$ cm/s. This estimate confirms that solid density, and thus elevated pressure, still exist at $\Delta t \sim 1$ ps, and simultaneously supports the argument that the reflectivity decrease observed at $\Delta t > 5$ ps corresponds to the expansion of initially pressurized material. Rothenberg[45] has measured such a pressure release time in picosecond-irradiated solid silicon using time-resolved photothermal deflection spectroscopy.

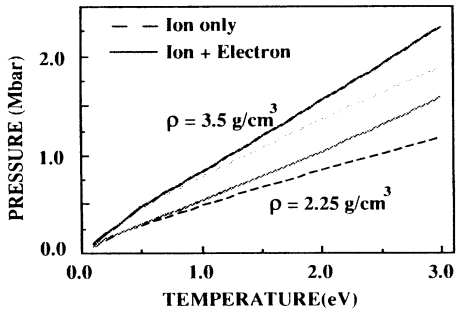

FIG. 10. Effective pressure of carbon sample following constant volume heating at density of graphite (2.25 g/cm^3) or diamond (3.5 g/cm^3), calculated using approximate equation of state formulas described in Ref. 44. Dashed curves include the dominant ionic contribution only; solid curves include both ionic and Thomas-Fermi electronic contributions to pressure.

V. DRUDE DIELECTRIC FUNCTION OF LIQUID CARBON

We now analyze in detail the measured optical properties of the fluid state. This analysis is compared directly to optical properties predicted by molecular dynamics simulations, and to pulsed electrical measurements of dc conductivity of liquid carbon.

The dielectric function of most liquid metals is well described by a Drude function:[46]

$$\epsilon(\omega) = \epsilon_{1c} - \frac{\omega_p^2 \tau^2}{1+\omega^2\tau^2} + i\epsilon_{2c} + i\frac{\omega_p^2 \tau}{\omega(1+\omega^2\tau^2)} . \quad (4)$$

Success in fitting the optical properties of the related column IV liquid metals Si,[25,43] Ge,[47] and Sn,[47] with this model especially motivates its application to liquid carbon. Usually the polarizability (ϵ_{1c}) and residual interband absorption (ϵ_{2c}) of the ionic cores can be neglected ($\epsilon_{1c} = 1$, $\epsilon_{2c} = 0$), leaving the free electron plasma frequency $\omega_p^2 = 4\pi n_e e^2/m$ (n_e = electron density, m = free electron mass) and relaxation time τ as the dominant parameters which determine surface reflectivity. We shall follow this simplifying assumption initially, then later examine the effect of introducing finite core dielectric parameters. Full determination of the Drude parameters ω_p and τ requires at least two independent measurements; measurements at steep incidence angle usually provide the greatest precision in determining $\epsilon(\omega)$. Our measurements can be summarized in two categories: (1) the normal incidence reflectivity spectrum $R(h\nu)$ over the range $1.77 \le h\nu \le 4.0$ eV (see Figs. 6–8) and (2) oblique incidence ($\theta = 50°$) s- and p-polarized reflectivity at $h\nu = 2.0$ eV [e.g., Figs. 4(a) and 4(d)]. Measurements at $\Delta t \sim 1$ ps at each of several pump fluences are used for the analysis. Any choice of Drude parameters must be consistent with all measurements for a given pump fluence.

Figure 11 plots the normal incidence reflectivity spectrum at $\Delta t \sim 1$ ps for two fluences (large solid squares: 0.5 J/cm^2; open squares: 2.0 J/cm^2), as gleaned from the data in Figs. 6–8. This data is compared to the measured reflectivity spectra of solid graphite (solid curve), diamond (crosses), and liquid silicon (open circles). The measured reflectivity decreases monotonically with increasing photon energy $h\nu$, and equals or exceeds the reflectivity of the corresponding solids throughout the probed frequency range. At visible frequencies the measured reflectivity increases with pump fluence up to a maximum of about 0.5, although at $h\nu = 4.0$ eV, reflectivity was independent of fluence within experimental error. The first column of Fig. 12 plots the measured s- and p-polarized oblique incidence reflectivity at $h\nu = 2.0$ eV, $\Delta t \sim 1$ ps, at $F = 0.5$ J/cm^2, compared to the normal incidence reflectivity at the same probe wavelength.

The remaining curves in Figs. 11 and 12 are theoretical models of the reflectivity spectrum, which we now discuss

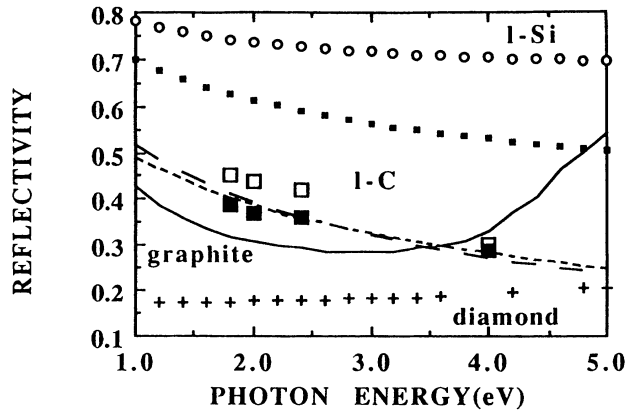

FIG. 11. Normal incidence reflectivity spectra of crystalline diamond (Ref. 27) (crosses); crystalline pyrolytic graphite (Ref. 26) (solid curve); carbon measured at $\Delta t \sim 1$ ps after a femtosecond melting of graphite with pulse of 0.5 J/cm^2 (large solid squares) or 2.0 J/cm^2 (large open squares); liquid carbon calculated using Drude parameters $\omega_p = 3.5\times10^{16}$ s^{-1}, $\tau = 0.25\times10^{-16}$ s (dotted curve) and $\omega_p = 1.6\times10^{16}$ s^{-1}, $\tau = 0.9\times10^{-16}$ s (dashed curve); liquid carbon calculated from molecular dynamics simulation at atmospheric pressure (Ref. 6) (small solid squares); liquid silicon measured by ellipsometric methods (Ref. 25) (open circles).

further. The small solid squares in Fig. 11 represent a reflectivity spectrum $R(\omega)$ extracted from the conductivity function $\sigma(\omega)$ derived by Galli *et al.*[6] from a molecular dynamics simulation of liquid carbon [see Fig. 2 of Ref. 6(a)] for the following conditions: low pressure $P \sim 1$ atm, $T_e = T_i = 5000$ K, density $\rho = 2.0$ g/cm^3. To obtain this $R(\omega)$, $\mathrm{Im}\sigma(\omega)$ was derived by Kramers-Kronig transformation of $\mathrm{Re}\sigma(\omega)$ given by Galli *et al.*;[6] then $\epsilon(\omega)$, expressed in terms of complex conductivity,

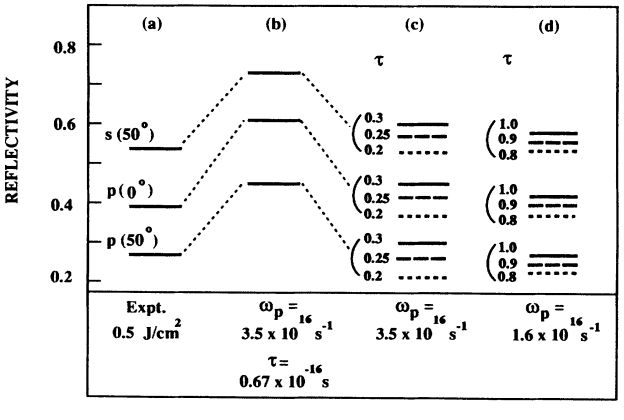

FIG. 12. Oblique ($\theta = 50°$) incidence, *s*- and *p*-polarized, and normal ($\theta = 0°$) incidence reflectivity of liquid carbon at photon energy 2 eV. (a) measured at $\Delta t \sim 1$ ps after a femtosecond melting of graphite with pulse of 0.5 J/cm^2; (b) calculated from molecular dynamics simulation at atmospheric pressure (Ref. 6); (c) calculated using Drude parameters $\omega_p = 3.5\times10^{16}$ s^{-1}, $\tau = 0.2$, 0.25, 0.3×10^{-16} s; (d) calculated using Drude parameters $\omega_p = 1.6\times10^{16}$ s^{-1}, $\tau = 0.8$, 0.9, 1.0×10^{-16} s.

was used to derive $R(\omega)$. Alternatively, a nearly identical $R(\omega)$ was obtained over the frequency range of our data by fitting $\mathrm{Re}\sigma(\omega)$ to a Drude function $\omega_p^2\tau/4\pi(1+\omega^2\tau^2)$, then substituting the resulting best fit Drude parameters $\omega_p = 3.5\times10^{16}$ s^{-1} and $\tau = 0.67\times10^{-16}$ s^{-1}, into the dielectric function Eq. (4) with $\epsilon_{1c} = 1$, $\epsilon_{2c} = 0$. Physically, the best fit ω_p corresponds to $n_e = 3.8\times10^{23}$ cm^{-3} (assuming a free electron mass), very close to four times the atomic density $n_a = 1\times10^{23}$ cm^{-3} corresponding to $\rho = 2.26$ g/cm^3, implying a nearly quadrivalent metal. The best fit τ implies a mean-free path $l = v_F\tau = 1.8$ Å (v_F = Fermi velocity $= 2.6\times10^8$ cm/s), close to the average interatomic spacing $n_a^{-1/3} = 2.1$ Å. The second column of Fig. 12 shows the oblique incidence reflectivity calculated from Fresnel's equations, using the same dielectric function.

The calculated reflectivity is approximately 50% higher than the observed reflectivity (Figs. 11 and 12), well outside of experimental inaccuracy. We therefore consider possible causes of this significant discrepancy. One possibility is that core dielectric terms must be included along with the best fit Drude parameters. However, introducing a core polarizability as large as that of solid graphite ($\epsilon_{1c} = 4.5$) together with the best-fit Drude parameters cited above yields $R(2\text{ eV}) = 0.58$ and $R(4\text{ eV}) = 0.45$, still well above the observed values. We have investigated systematically combinations of core dielectric terms in the ranges $1 \le \epsilon_{1c} \le 4.5$ and $0 \le \epsilon_{2c} \le 4.0$, and find generally that core dielectric terms cannot explain the discrepancy shown. We must conclude that the Drude parameters themselves are different from the values extracted from the simulations of Galli *et al.*,[6] or that the Drude function itself does not adequately describe the properties of carbon 1 ps after photoexcitation. Close agreement should not necessarily be expected, because our experiment probes a sample at high pressure, and densities close to those of the initial solids (graphite: 2.26 g/cm^3; diamond: 3.5 g/cm^3). The discrepancy provides motivation for further simulations of the electronic properties of liquid carbon under conditions closer to those of the experiment. In fact, a molecular dynamics simulation at high pressure has been reported,[6(b)] but to our knowledge electrical properties were not derived. In the current absence of such simulations, we consider what revisions in the dielectric function can better explain the reflectivity data.

The dotted curve in Fig. 11 shows a greatly improved fit to $R(\omega)$ at $F = 0.5$ J/cm^2 obtained by reducing the value of τ from 0.67 to 0.25×10^{-16} s, while retaining other parameters ($\omega_p = 3.5\times10^{16}$ s^{-1}, $\epsilon_{1c} = 1$, $\epsilon_{2c} = 0$) corresponding to a simple nearly quadrivalent Drude metal. The third column of Fig. 12 shows that the oblique incidence reflectivity at $F = 0.5$ J/cm^2 is also explained almost perfectly by this dielectric function, and that slightly larger (0.3×10^{-16} s) or smaller (0.2×10^{-16} s) values of τ significantly worsen the fit. Nevertheless this fit is not unique. The dashed curve in Fig. 11 and the fourth column of Fig. 12 show that a fit of nearly equal quality is obtained by decreasing ω_p to 1.6×10^{16} s^{-1}, corresponding to a monovalent ($n_e = 1\times10^{23}$ cm^{-3}) metal, and increasing τ to 0.9×10^{-16} s. In fact a family of

(ω_p,τ) pairs in between these two extremes, plotted as a line in the (ω_p,τ) plane in Fig. 13(a), provide satisfactory fits to our reflectance data for $F=0.5$ and 2 J/cm^2. Fits of similar quality are obtained for the data at other fluences. Thus the individual Drude parameters are not uniquely determined by our current data. On the other hand, the line in Fig. 13(a) determines the *product* $\omega_p\tau$ and the *dc resistivity* $\rho_{dc}=4\pi/\omega_p^2\tau$ to within relatively narrow ranges, as shown in Fig. 13(b) (e.g., $1<\omega_p\tau<1.6$ and $400<\rho_{dc}<500$ $\mu\Omega$ cm for 0.5 J/cm^2). Finally Fig. 13(c) shows the dependence of the optically determined

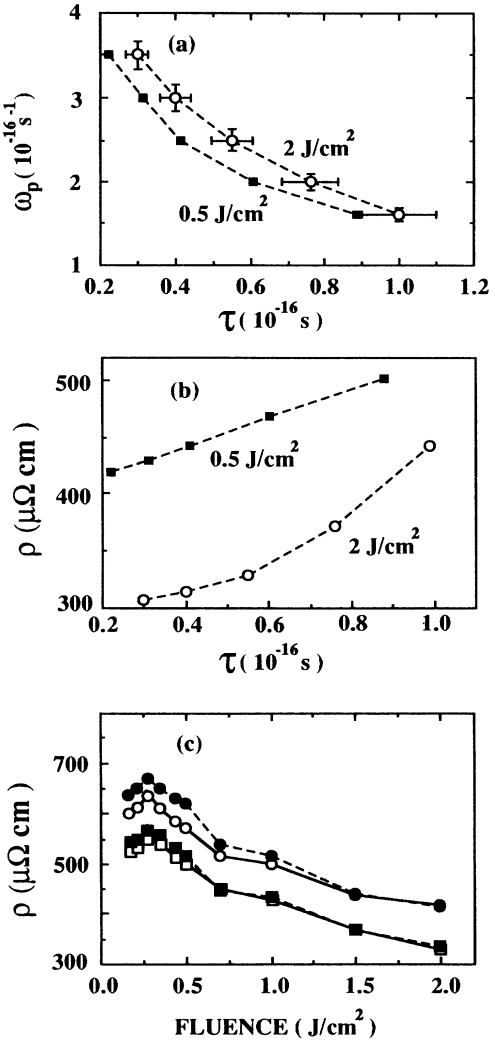

FIG. 13. (a) Family of Drude parameters ω_p and τ which provide satisfactory fits to carbon reflectance data at $\Delta t\sim 1$ ps after femtosecond melting pulse at 0.5 and 2.0 J/cm^2; (b) dc resistivity values $4\pi/\omega_p^2\tau$ corresponding to family of Drude parameters in (a); (c) dependence of optically determined resistivity on pump fluence, showing four different data analyses assuming ω_p constant at either 1.6×10^{16} s^{-1} (open circles) or 3.5×10^{16} s^{-1} (open squares) and τ variable with increasing fluence; or, conversely, τ constant at either 0.3×10^{-16} s (solid squares) or 1.0×10^{-16} s (solid circles), and ω_p variable with increasing fluence.

ρ_{dc} on pump fluence. Because ω_p and τ may individually vary with fluence in a range of possible ways, four plots of ρ_{dc} illustrating the extreme cases are shown in Fig. 13(c): ω_p constant (at either 1.6 or 3.5×10^{16} s^{-1}) and τ variable with increasing fluence; or, conversely, τ constant (at either 0.3 or 1.0×10^{-16} s), and ω_p variable with increasing fluence. In all cases, ρ_{dc} decreases from 625 ± 75 $\mu\Omega$ cm slightly above the melting fluence to 375 ± 75 $\mu\Omega$ cm at tenfold higher fluence. For $0.13<F<0.3$ J/cm^2, the reflectance data was first corrected for the incomplete overlap of the melted area with the probe spot, using the data in Fig. 1. The slight increase in ρ for $F<0.25$ J/cm^2 falls within experimental error. The trend in ρ contrasts with the usual increase of ρ with temperature in metals, but follows the usual decrease of ρ with pressure, as discussed further below.

Table I compares our optically derived Drude parameters and dc resistivity with optical-derived parameters of the other column IV liquid metals (measured at atmospheric pressure slightly above their respective melting points), and with pulsed electrical measurements and theoretical simulations for liquid carbon. Our product $\omega_p\tau\sim1$ is significantly smaller than for the other column IV liquid metals, indicating an unusually strongly damped electron plasma and strong electron localization. Similarly, the optically determined ρ_{dc} is significantly higher than those of the other metals. The *l*-C values are consistent qualitatively with the trends of decreasing $\omega_p\tau$ and increasing ρ_{dc} as atomic size decreases in column IV. The unusually large size of the changes between *l*-Si and *l*-C is consistent with the much higher temperature required to melt carbon, which in turn strongly reduces the electron collision time τ. Nevertheless, the unusually small numerical values of τ ($0.3<\tau<1.0\times10^{-16}$ s) for *l*-C compared to optically determined τ values in *l*-Si (2.1×10^{-16} s), *l*-Ge (2.5×10^{-16} s), and *l*-Sn (3.5×10^{-16} s) warrant further comment, since they imply electron mean free paths $l\sim v_F\tau$ in the range $0.8<l<1.7$ Å, which are actually somewhat *smaller* than the average interatomic spacing ($N^{-1/3}\sim2$ Å). $N^{-1/3}$ should set an approximate lower limit on the path between electron scattering events, leading to "saturation" of ρ_{dc} and τ with increasing temperature,[48] as has been observed in aluminum under short pulse heating conditions.[49] A possible physical mechanism yielding l slightly less than $N^{-1/3}$ might be collisions within localized carbon molecules containing small angle bonds. Alternatively, a residual population of anomalously hot electrons with $v>v_F$ would have mean-free paths larger than the range indicated above. On the other hand, in view of the phenomenological nature of the Drude model, the precise value of τ should probably not be interpreted too literally, as long as $v_F\tau$ saturates in the vicinity of $N^{-1/3}$. Indeed the fluence dependence shown in Fig. 13(c) is fully consistent with a saturated resistivity above the melting fluence, since resistivity does not increase as fluence increases above F_m (with the possible exception of a slight increase in a narrow range just above F_m). In fact, rather than leveling off, resistivity actually *decreases* with approximately $F^{-0.6}$ dependence. The decrease in ρ prob-

TABLE I. Summary of measurements and calculations of Drude parameters and dc resistivity in column IV liquid metals.

Liquid	Pressure (bars)	Temperature (K)	$\omega_p\tau$	ρ_{dc} ($\mu\Omega$ cm)	Method	Reference
Sn	1	1130	8	60	cw ellipsometry	Hodgson (Ref. 47)
Ge	1	1270	6	75	cw ellipsometry	Hodgson (Ref. 47)
Si	1	1800	5.6	80	cw ellipsometry	Shvarev *et al.* (Ref. 43)
	1	1800	5.3	85	Picosecond reflectance	Li and Fauchet (Ref. 25)
C	$\sim 0.3\times 10^6$	~ 6000	1–1.6	625±75	Femtosecond reflectance	This work
	4×10^3	~ 5000		1000	Ohmic heating	Gathers *et al.* [Ref. 14(a)]
	1	~ 4500		30–70	Ohmic heating	Heremans *et al.* (Ref. 4)
	1	5000	2.3	140±28	Molecular dynamics simulation	Galli *et al.* [Ref. 6(a)]

ably has multiple causes, including increasing ionization (i.e., increasing ω_p, even at constant τ), and an approach to high temperature plasma behavior, in which resistivity is increasingly determined by Coulomb scattering,[50] and scales as $T^{-3/2}$.

The range of Drude parameters cited above corresponds to a range of possible electronic and molecular structures. The smaller ω_p (1.6×10^{16} s^{-1}) corresponds to a monovalent metal, implying that three of the four valence electrons of carbon are involved in covalent bonding. Indeed the molecular dynamics simulation of Galli *et al.*,[6] although consistent with a quadrivalent electronic structure at low pressure, nevertheless shows prevalent clusters and chainlike molecular structures in the liquid state. On the other hand, the other column IV liquid metals are all quadrivalent metals.[25,47] The current results provide no firm basis for distinguishing between these two pictures, or an intermediate version. Molecular dynamics simulations of the electronic properties at elevated pressure, together with extended femtosecond ellipsometric measurements at very steep probe incidence angles and vacuum ultraviolet probe frequencies will narrow the uncertainty considerably, and possibly detect variations from Drude-like optical properties. Whichever of these interpretations proves ultimately correct, the current experiments show clearly that liquid carbon is a resistively saturated material, for which the "free electron" Drude model and the attribution "metal" are at the limits of their validity.

Comparison of our optically determined resistivity with pulsed electrical heating measurements of liquid carbon (see Table I) also provides physical insight. The measurements which most closely approximate our pressure-temperature conditions involve pulsed ohmic heating of vitreous[14(c)] or glassy carbon[14(d)] to temperatures up to 6000 K under 2–4 kbar rare gas pressure. Melt resistivities $\rho\sim 1000$ $\mu\Omega$ cm were reported from these measurements, which is very consistent with our optically determined values just above F_m. In fact the somewhat smaller values obtained in our experiment are fully consistent with the higher sample compression under femtosecond excitation, which suppresses the amplitude of ionic vibrational motion responsible for electron scattering and resistivity. Indeed clear evidence of volume expansion was obtained in the pulsed ohmic heating measurements,[14(c)] and was taken into account in determining the resistivity. On the other hand, recent measurements[4] and calculations[6,7] at ambient atmospheric pressure have yielded much smaller resistivities than obtained in our experiment. Heremans *et al.*[4] reported resistivity $30<\rho<70$ $\mu\Omega$ cm based on resistance measurements of ohmically heated pyrolytic graphite fibers at atmospheric pressure. Two theoretical simulations performed after this experiment yielded resistivities of 140 $\mu\Omega$ cm,[6] and 80 $\mu\Omega$ cm[7]. Volume expansion upon melting was neglected in analyzing the measured resistance, which, if present to the degree observed in Ref. 14(c), could raise the reported resistivity by as much as a factor of 2. Nevertheless, even with this correction the values would still fall significantly below ours. The lower sample pressure compared to our conditions is expected to yield higher, rather than lower resistivity (in the absence of phase transitions). Thus other causes of the discrepancy with our measurements must be sought. One possibility is that the nature of the material is very different at atmospheric pressure. Indeed, a number of independent experiments in which graphite was melted in atmospheres of pressurized inert gases have agreed that the solid-vapor-liquid triple point occurs at ~ 110 atm. pressure.[3(c),51] Thus according to these investigators, an equilibrated liquid phase of carbon does not even exist at atmospheric pressure. It is therefore conceivable that atmospheric pressure experiments measure a qualitatively different phase of carbon than high pressure experiments. Reconciliation of the various pulsed ohmic heating experiments is complicated by their use of different starting forms of carbon, and by the lack (to our knowledge) of measurements on a single type of starting sample at pressures both above and below 110 atm. In addition, the reported electrical resistivity of the heated phase sometimes depends on prior history (e.g., heat treatment) of the starting solid. These ambiguities would be clarified by performing ohmic heating experiments on well-characterized pyrolytic graphite fibers, glassy carbon, vitreous carbon, and perhaps other solid carbon forms at systematically varied pressures ranging from 1 bar to several kbar. In summary, our optically determined resistivity agrees very well with pulsed electrical measurements reported for carbon samples melted at pressures well above the widely accepted triple point pressure of

110 atm,[14] but significantly exceeds reported measurements[4] and calculations[6,7] of resistivity for low pressure samples.

VI. CONCLUSIONS

Femtosecond melting experiments measure the optical and electronic properties of refractory condensed materials in quantitative detail at extremes of pressure and temperature inaccessible by other experimental methods. We have presented a comprehensive study of the optical properties of liquid carbon produced by femtosecond excitation of pyrolytic graphite and diamond above critical melting fluences of 0.13 J/cm^2 and 0.6 J/cm^2, respectively. All evidence suggests that both samples melt, reach nearly common electron-lattice temperature and steady state visible reflectance higher than the starting solids within 1 ps, before the release of internal pressure and hydrodynamic expansion distort the optical properties of the surface. A careful analysis of fluence-dependent reflectance at $\Delta t > 1$ ps and fluence-dependent damage morphology shows that surface expansion strongly attenuates surface reflectivity within a few picoseconds of femtosecond irradiation at all fluences above the critical melting fluence. A Drude model fit of the measured reflectance spectrum at $\Delta t \sim 1$ ps shows liquid carbon to be a resistively saturated metal under femtosecond melting conditions, consistent with dc resistivity measurements made on carbon samples melted by pulsed ohmic heating in an inert, pressurized atmosphere.

This work points to a number of areas for additional research. The pressure dependence of the electrical properties of liquid carbon should be clarified by theoretical simulations at high pressure and by pulsed electrical measurements on well-characterized samples at systematically varied pressures between 1 bar and several kbar. Femtosecond experiments can be improved by using probe pulses at vacuum ultraviolet wavelengths and steep incidence angles, in order to probe the plasma edge more accurately and determine individual Drude parameters more precisely than has been possible in this work. Significant deviations from Drude-like behavior might also be detected. The degree of equilibration following femtosecond excitation can be further clarified by dynamical simulations which start with graphite and/or diamond crystalline structures, and by more extensive comparison of the femtosecond time-resolved reflectance of less refractory materials with independently measured optical properties of the equilibrated liquid phases. Finally, in a larger context, femtosecond spectroscopy provides a promising method for optically characterizing a wide range of condensed, refractory materials in previously inaccessible pressure and temperature regimes characteristic of planetary and stellar interiors.

ACKNOWLEDGMENTS

This research was supported by the National Science Foundation (Grant No. DMR-8858388), the Robert A. Welch Foundation (Grant F-1038), and the Air Force Office of Scientific Research (Contract F49620-89-C-0044). We acknowledge helpful discussions with J. C. Thompson and N. Bloembergen.

*Present address: Bellcore, Red Bank, NJ 07701.

[1]A. Ludwig, Z. Electrochem. **8**, 273 (1902).

[2](a) F. P. Bundy, Physica (Amsterdam) **156A**, 169 (1989); (b) J. Geophys. Res. **85**, 6930 (1980).

[3](a) A. G. Whittaker, P. L. Kitner, L. S. Nelson, and N. Richardson (unpublished); (b) M. A. Scheindlin, Mater. Res. Soc. Symp. Proc. **22**, 33 (1984); (c) N. A. Gokchen, E. T. Chang, T. M. Poston, and D. J. Spencer, High Temp. Sci. **8**, 81 (1976).

[4]J. Heremans, C. H. Olk, G. L. Eesley, J. Steinbeck, and G. Dresselhaus, Phys. Rev. Lett. **60**, 452 (1988).

[5]J. Steinbeck, G. Braunstein, M. S. Dresselhaus, T. Venkatesan, and D. C. Jacobson, J. Appl. Phys. **58**, 4374 (1985); **64**, 1802 (1988).

[6](a) G. Galli, R. M. Martin, R. Car, and M. Parrinello, Phys. Rev. Lett. **63**, 988 (1989); (b) Science **250**, 1547 (1990); (c) Phys. Rev. B **42**, 7470 (1990).

[7]M. W. C. Dharma-wardana and Francois Perrot, Phys. Rev. Lett. **65**, 76 (1990).

[8]A. M. Malvezzi, N. Bloembergen, and C. Y. Huang, Phys. Rev. Lett. **57**, 146 (1986).

[9]E. A. Chauchard, C. E. Lee, and C. Y. Huang, Appl. Phys. Lett. **50**, 812 (1987).

[10]D. H. Reitze, X. Wang, H. Ahn, and M. C. Downer, Phys. Rev. B **40**, 11 986 (1989).

[11](a) D. H. Reitze, H. Ahn, X. Wang, and M. C. Downer, in *Ultrafast Phenomena VII,* edited by C. B. Harris, E. P. Ippen, G. A. Mourou, and A. Zewail (Springer-Verlag, Berlin, 1990); (b) D. H. Reitze, Ph.D. dissertation, University of Texas at Austin, 1990.

[12]T. Venkatesan, D. C. Jacobson, J. M. Gibson, B. S. Elman, G. Braunstein, M. S. Dresselhaus, and G. Dresselhaus, Phys. Rev. Lett. **53**, 360 (1984).

[13]J. S. Speck, J. Steinbeck, and M. S. Dresselhaus, J. Mater. Res. **5**, 980 (1990).

[14](a) A. C. Mitchell, J. W. Shaner, and R. N. Keller, Physica **139**, 386 (1986); (b) G. R. Gathers, J. W. Shaner, and R. L. Brier, Rev. Sci. Instrum. **47**, 471 (1976); (c) G. R. Gathers, J. W. Shaner, and D. A. Young (unpublished); (d) J. W. Shaner, Bull. Am. Phys. Soc. **32**, 607 (1987).

[15](a) J. W. Shaner, J. M. Brown, C. A. Swenson, and R. G. McQueen, J. Phys. C **8**, 235 (1984); (b) J. Kleinman, R. B. Heimann, D. Hawken, and N. M. Salansky, J. Appl. Phys. **56**, 1440 (1984).

[16]M. Ross, Nature (London) **292**, 435 (1981).

[17]D. A. Young and R. Groover, in *Shock Waves in Condensed Matter,* edited by S. C. Schmidt and M. C. Holmes (Elsevier, New York, 1988), p. 131.

[18]M. S. Weathers and W. A. Bassett, Phys. Chem. Miner. **15**, 105 (1987).

[19]J. S. Dickey, W. A. Bassett, J. M. Bird, and M. S. Weathers, Geology **11**, 219 (1983).

[20]A. Ferraz and N. H. March, Phys. Chem. Liq. **8**, 289 (1979).

[21]M. C. Downer, R. L. Fork, and C. V. Shank, J. Opt. Soc. Am. B **2**, 595 (1985).

[22]H. W. K. Tom, G. D. Aumiller, and C. H. Brito-Cruz, Phys. Rev. Lett. **60**, 1438 (1988).

[23]K. Seibert, G. C. Cho, W. Kütt, H. Kurz, D. H. Reitze, J. I.

Dadap, H. Ahn, M. C. Downer, and A. M. Malvezzi, Phys. Rev. B **42**, 2842 (1990).

[24]N. H. March, *Liquid Metals* (Cambridge University Press, Cambridge, England, 1990).

[25]K. D. Li and P. Fauchet, Appl. Phys. Lett. **51**, 1747 (1987).

[26](a) B. T. Kelly, *The Physics of Graphite* (Applied Science, London, 1980); (b) L. G. Johnson and G. Dresselhaus, Phys. Rev. B **7**, 2275 (1973); (c) E. A. Taft and H. R. Philipp, Phys. Rev. **138**, 197 (1965).

[27](a) G. S. Painter, D. E. Ellis, and A. R. Lubinsky, Phys. Rev. B **4**, 3610 (1971); (b) H. R. Philipp and E. A. Taft, Phys. Rev. **136**, A1445 (1964); (c) R. A. Roberts and W. C. Walker, *ibid.* **161**, 730 (1967).

[28]C. V. Shank, R. Yen, and C. V. Hirlimann, Phys. Rev. Lett. **50**, 454 (1983).

[29]R. L. Fork, B. I. Greene, and C. V. Shank, Appl. Phys. Lett. **38**, 671 (1981).

[30]W. M. Wood, G. Focht, and M. C. Downer, Opt. Lett. **13**, 984 (1988).

[31](a) M. F. Becker, R. M. Walser, Y. K. Jhee, and D. Y. Sheng, SPIE **322**, 93 (1982); (b) L. W. Boyd, S. C. Moss, T. F. Boggess, and A. L. Smirl, Appl. Phys. Lett. **45**, 80 (1984); (c) A. M. Malvezzi, H. Kurz, N. Bloembergen, in *Energy Beam-Solid Interactions and Transient Thermal Processing,* edited by D. K. Biegelsen, G. A. Rozgonyi, and C. V. Shank (Materials Research Society, Pittsburgh, 1985).

[32]R. L. Fork, C. V. Shank, C. Hirlimann, R. Yen, and W. J. Tomlinson, Opt. Lett. **8**, 1 (1983).

[33]J. M. Liu, Opt. Lett. **7**, 196 (1980).

[34]J. I. Dadap, D. H. Reitze, G. B. Focht, and M. C. Downer, Opt. Lett. **16**, 499 (1991).

[35]R. Fedosejevs, R. Ottmann, R. Sigel, G. Kühnle, S. Szatmari, and F. P. Schäfer, Phys. Rev. Lett. **64**, 1250 (1990).

[36](a) H. M. Milchberg and R. R. Freeman, J. Opt. Soc. Am. B **6**, 1351 (1989); (b) H. M. Milchberg, R. R. Freeman, S. C. Davey, and R. M. More, Phys. Rev. Lett. **61**, 2364 (1988).

[37]N. Bloembergen, in *Beam-Solid Interactions and Phase Transformations,* edited by H. Kurz, G. L. Olsen, and J. M. Poate (Materials Research Society, Pittsburgh, 1986), p. 3.

[38]Y. B. Zeldovich and Y. P. Raizer, *Physics of Shock Waves and High Temperature Hydrodynamic Phenomena* (Academic, New York, 1966).

[39]R. M. More, Adv. At. Mol. Phys. **21**, 305 (1985).

[40]S. D. Brorson, A. Kazeroonian, J. S. Moodera, D. W. Face, T. K. Cheng, E. P. Ippen, M. S. Dresselhaus, and G. Dresselhaus, Phys. Rev. Lett. **64**, 2172 (1990).

[41]F. E. Doany and D. Grischkowsky, Appl. Phys. Lett. **52**, 36 (1988).

[42]P. M. Fauchet and D. Hulin, J. Opt. Soc. Am. B **6**, 1024 (1989).

[43]K. M. Shvarev, B. A. Baum, and P. V. Gel'd, Fiz. Tverd. Tela (Leningrad) **16**, 3246 (1974) [Sov. Phys. Solid State **16**, 2111 (1975)].

[44]R. M. More, K. H. Warren, D. A. Young, and G. B. Zimmerman, Phys. Fluids **31**, 3059 (1988).

[45]J. E. Rothenberg, Opt. Lett. **13**, 713 (1988).

[46]T. E. Faber, *Introduction to the Theory of Liquid Metals* (Cambridge University Press, Cambridge, England, 1972).

[47](a) J. N. Hodgson, Philos. Mag. **6**, 509 (1961); (b) N. R. Comins, *ibid.* **25**, 817 (1972).

[48]N. F. Mott, *Metal-Insulator Transitions* (Taylor and Francis, London, 1974).

[49]H. M. Milchberg, R. R. Freeman, S. C. Davey, and R. M. More, Phys. Rev. Lett. **61**, 2364 (1988).

[50]L. Spitzer, Jr., *Physics of Fully Ionized Gases* (Wiley, New York, 1962).

[51](a) G. J. Schoessow, Phys. Rev. Lett. **21**, 738 (1968); (b) N. S. Fateeva and L. F. Vereshchagin, Pis'ma Zh. Eksp. Teor. Fiz. **13**, 157 (1971) [JETP Lett. **13**, 110 (1971)]; (c) D. M. Haaland (unpublished).

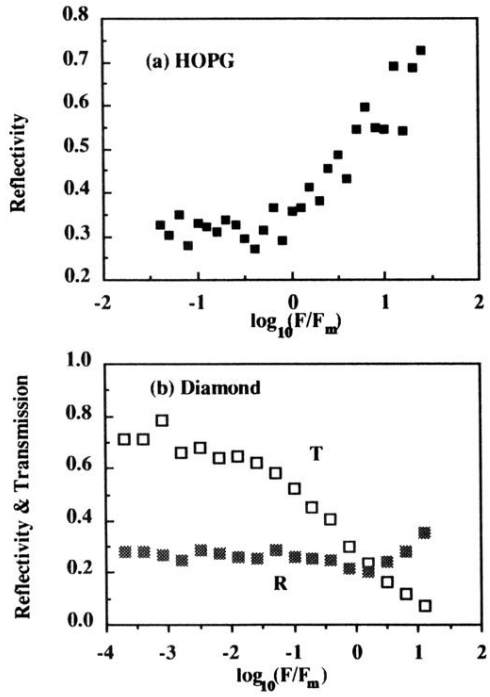

FIG. 3. (a) Self-reflectivity of 90-fs, 620-nm pulses normally incident on HOPG as a function of fluence F normalized to the critical melting fluence F_m. (b) Fluence dependent self-reflectivity and transmission of 90-fs, 620-nm pulses normally incident on diamond.

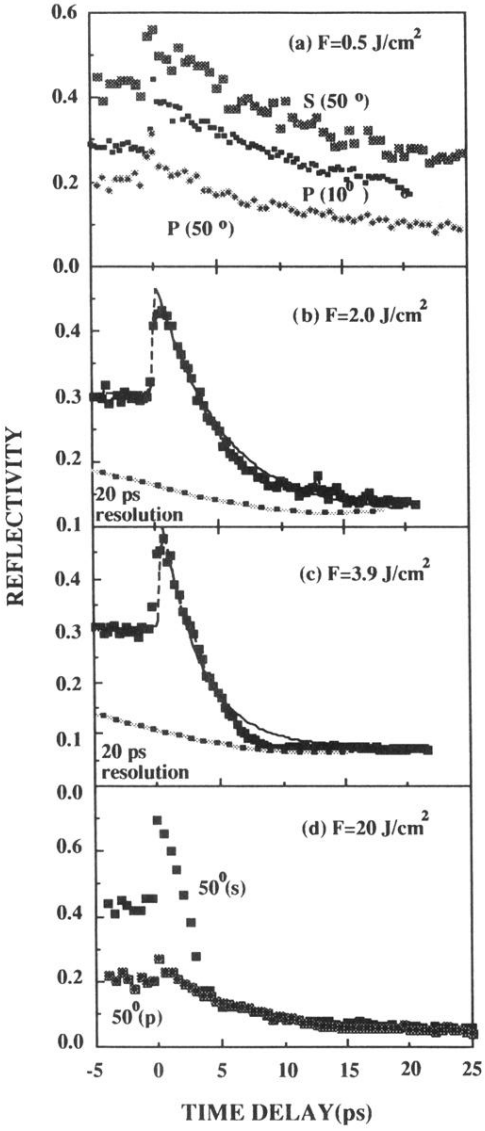

FIG. 4. Femtosecond time-resolved reflectivity of HOPG. (a) Excitation at pump fluence $F = 0.5$ J/cm^2, probe at 620 nm, comparing 50° incident angle s and p polarized reflectivity, and near-normal incidence reflectivity. (b) Near-normal incidence 620-nm reflectivity at $F = 2.0$ J/cm^2; dashed line shows convolution of data with 20-ps pump and probe pulses. (c) Same with $F = 3.9$ J/cm^2. (d) Excitation at 20 J/cm^2, probe at 620 nm, comparing 50° incident angle s and p polarized reflectivity. Vertical scales on all panels denote absolute reflectivity.